Nuclear Instruments and Methods in Physics Research A 788 (2015) 146–153

Contents lists available at ScienceDirect

Nuclear Instruments and Methods in Physics Research A

journal homepage: www.elsevier.com/locate/nima

Comparative analysis of pulse shape discrimination methods in a ^{6}Li loaded plastic scintillator

Matthew J.I. Balmer [a,*], Kelum A.A. Gamage [a], Graeme C. Taylor [b]

[a] Department of Engineering, Lancaster University, LA1 4YR, UK
[b] Neutron Metrology Group, National Physical Laboratory, Teddington, TW11 0LW, UK

ARTICLE INFO

Article history:
Received 8 December 2014
Received in revised form
26 March 2015
Accepted 31 March 2015
Available online 8 April 2015

Keywords:
Plastic scintillator
Digital pulse shape discrimination
Figure of merit (FOM)
Thermal neutron detection

ABSTRACT

Three algorithms for discriminating between fast neutrons, thermal neutrons and gamma rays in a ^{6}Li loaded plastic scintillator have been compared. Following a literature review of existing pulse shape discrimination techniques, the performance of the charge comparison method, triangular filtering and frequency gradient analysis were investigated in this work. The scintillator was exposed to three different mixed gamma/neutron radiation fields. The figure of merit of neutron/gamma separation was investigated over a broad energy range, as well as for the neutron capture energy region. After optimisation, all three methods were found to perform similarly in terms of neutron/gamma separation.

1. Introduction

Scintillators loaded with a high neutron capture cross-section isotope enable detection of not only fast neutrons, but also thermal neutrons. Recently, plastic scintillators with a ^{6}Li loading have been developed, with the ability to discriminate events between thermal neutron, fast neutron and gamma interactions [1]. When compared to low flash point loaded liquid scintillators, the advantages of easy to machine plastics are obvious.

When a neutron interacts in a scintillator, its primary method of energy loss is through elastic scattering with a proton. The recoil of this proton excites π-electrons within the molecular structure of the scintillator, raising the π-electrons from their ground state to either a singlet, S_i, or triplet state, T_i. The decay of π-electrons back to their ground state results in a prompt emission of photons, known as *fluorescence*. This *fast component* of the detected scintillation pulse typically occurs a few nanoseconds after the excitation. With the interaction of two π-electrons in the T_i state it is possible to be left with one in the S_0 state and one in the S_1 state. When this S_1 electron decays the photon emission is known as *slow fluorescence*. This produces the *slow component* of a scintillation pulse [2].

Heavier particles exhibit a greater rate of energy loss in a scintillator, due to their higher ionising densities resulting in pulses that decay more slowly by delayed fluorescence. Hence, by examining the differences in these pulse shapes, it is possible to determine the type of interacting particle.

If a neutron loses enough energy in a scintillator through elastic collisions, it is likely that it will be captured when a loading element is present in the scintillator. For a scintillator loaded with the high capture cross-section isotope ^{6}Li, the capture of the neutron results in the emission of two low atomic mass particles, shown as

$$^{1}n + {}^{6}Li \rightarrow t(2.73\ MeV) + \alpha(2.05\ MeV) \quad (1)$$

where t is tritium (^{3}H). The interaction of a gamma in a scintillator usually results in the Compton scattering of an electron. Therefore in a mixed radiation field, with a ^{6}Li loaded scintillator, four main particles (proton, α, tritium and an electron) are detected as a result of neutron scattering, neutron capture and gamma interactions respectively. The slow component of the scintillation pulse is proportional to the ionisation density of the interaction, so inspection of the slow component allows the discrimination of three primary interactions of neutrons and gammas in a scintillator. Theoretical models of these three pulse shapes are shown in Fig. 1.

This paper reviews prior research of pulse shape discrimination (PSD) techniques in a scintillator, including methods suitable for identification of neutron capture in a loaded scintillator. The three most promising techniques are compared using experimental methods.

2. A review of pulse shape discrimination for neutron detection in scintillators

Since the early application of PSD in liquid scintillators, the two primary methods of PSD were by zero crossing and charge comparison

* Corresponding author.
E-mail address: m.balmer@lancaster.ac.uk (M.J.I. Balmer).

http://dx.doi.org/10.1016/j.nima.2015.03.089

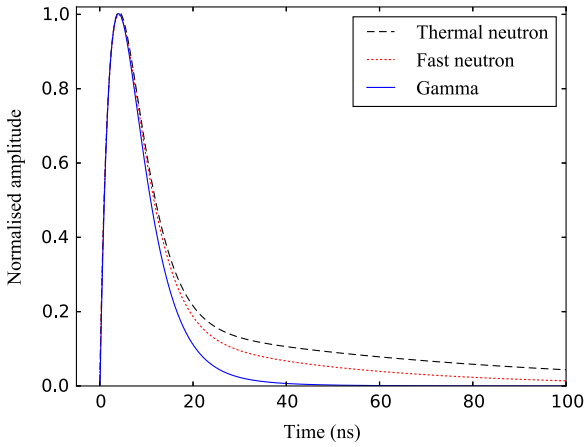

Fig. 1. Theoretical pulse shape of a fast neutron, captured thermal neutron and gamma interaction in a scintillator. Based on information presented by Zaitseva et al. [1]

techniques [3–5]. However, in the last decade, with the advances in semiconductor technology, there has been an increased focus towards digital approaches to PSD methodologies [6–9]. In particular advances in field-programmable gate array (FPGA) and analogue-to-digital converter (ADC) technologies now allow portable, real-time systems for neutron detection with scintillators.

2.1. Analogue techniques

The zero-crossing technique relies on external analogue circuitry to integrate, over time, the pulse detected by a photomultiplier tube (PMT). This integration is typically carried out by an RC circuit and the discrimination is based upon the time to reach a prescribed nominal voltage.

Arguably, the most commonly used PSD technique is charge integration. By integrating the pulse over two different time intervals (whole pulse (long), segment after peak (tail)) separation between particles can be observed. This simple algorithm lends itself well to implementation in the digital domain, for example removing complexity associated with analogue electronic hardware. Using recursive algorithms, both of these analogue techniques have been demonstrated as digital implementations [10].

2.2. Time domain

Pulse gradient analysis (PGA), first described by D'Mellow et al. [11], exploits the difference between the peak and a sample amplitude (after a given time) of a scintillation pulse. This method requires experimentation to find the optimum time interval between the peak and the sample amplitude. For optimum results, a finite impulse response (FIR) filter is recommended for use with this algorithm. Using a sample amplitude closer to the peak will improve pile-up capabilities as all information required to discriminate is recorded by this time.

Unknown particle interaction pulse shapes can be compared against a known set of pulse shapes in the time domain. Marrone at al. [12] presented an empirical method for comparison, this method has been compared with other PSD methods in the time domain [13]. By using a statistical technique to compare the difference between the theoretical pulse and the normalised unknown pulse, events can be classified as neutron or gamma events. Expanding further on these techniques, known for their pattern matching capabilities, artificial neural networks have been successfully deployed [9,14,15]. Typically time of flight (TOF) will be used to obtain a known pulse shape for a neutron/gamma interaction. However, this methodology is time consuming and would need to be repeated for any change to a system which could affect the pulse shape (cable, digitiser, amplifiers etc.). Recent investigations into pulse classification techniques highlight the possibility of foregoing TOF classification [16].

With the bulk of the signal processing performed in software, switching between PSD techniques can be used depending on the energy of the detected event [17]. A low-processing-intensive algorithm can be used for higher energies, whilst at lower energies, more computationally intensive algorithms can be used; thereby not impacting too much the overall throughput of the signal processing system.

Using triangular filtering techniques, Nakhostin demonstrated effective PSD down to 65 keVee [18]. It is worth noting that the results presented in this research were obtained using an ADC with a resolution of only 8 bits. Trapezoidal shaped filters have also been investigated [19].

2.3. Frequency domain

As previously noted FPGA technology has helped us to accelerate the growth of investigation into PSD in the digital domain, due to FPGA's inherent ability to perform fast parallel processing [20]. Indeed with modern FPGA technology boasting fast digital signal processing capabilities in a low cost package, some of the recursive techniques applied in the time domain demand very little of a modern FPGA based analyser. The recent investigations of PSD in the frequency domain lend themselves well to FPGA implementation [6,21–23]. Furthermore, frequency gradient analysis (FGA) has been shown to exhibit better noise rejection capabilities when compared to some techniques operating in the time domain [6,22–24].

To transform the detected pulse into the frequency domain, a frequency transform such as a Discrete Fourier Transform (DFT) or Discrete Wavelet Transform (DWT) can be used. The DFT has been favoured for PSD due to its lower computational overhead [22]. The difference between the zero frequency and the first frequency component of the Fourier transform is the mechanism which allows PSD to be realised using FGA.

3. Experimental method

The ^{6}Li loaded scintillator investigated in this work was provided by the Lawrence Livermore National Laboratory (LLNL), USA. The scintillator (denoted by the LLNL number 9023) had dimensions; 40 mm diameter and 25 mm thick [1].

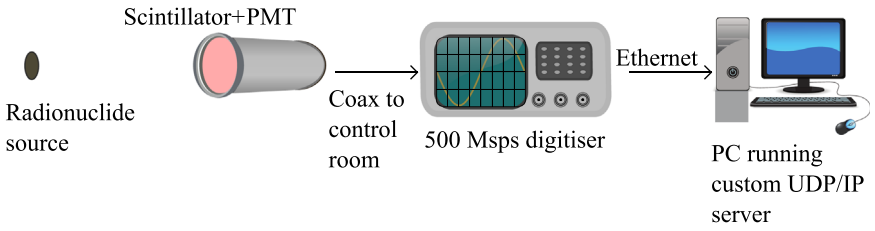

Fig. 2. Schematic diagram of the experimental setup.

The scintillator was coupled to an ET Enterprises 9214B PMT with Eljen EJ-550 optical grease. The scintillator was then enclosed in a light proof housing. The PMT was housed in a ET Enterprises B2F/RFI housing with a C638B tapered distribution voltage divider. The high voltage was set to −1200 V and connected to the PMT cathode. The PMT anode was connected to a Hybrid Instruments Ltd TOM digitiser system. The digitiser was configured to sample the raw pulses at a rate of 500 Msps (2 ns per ADC sample) with an effective resolution of 11 bits. The information for each triggered pulse consisted of 128 ADC samples. The data were sent to a UDP/IP server on a personal computer for recording. These samples were processed with a custom program written in Python. A schematic diagram of the hardware is shown in Fig. 2.

Previous research with the ^{6}Li loaded plastic scintillator has shown that the thermal capture cluster lies within the elastic neutron group [1]. The first investigation in this work was the capability to discriminate fast neutrons from gamma interactions in the scintillator. Three different mixed radiation fields were considered in this work, a ^{252}Cf (NPL reference number 4774) with a 12.7 cm diameter Bonner sphere surrounding the source, ^{241}AmBe (NPL reference number 1095) with a Pb cap to suppress low energy (60 keV) gamma detections in the scintillator, both unmoderated and surrounded by a 20.32 cm diameter Bonner sphere. The Bonner spheres were used for two of the sources to provide a higher thermal neutron fluence within the field. The unmoderated ^{241}AmBe field was chosen to contrast these fields with a low thermal content and higher fast neutron content. Each of the sources was located 1 m from the front face of the scintillator. The numbers of pulses recorded with each source are shown in Table 1.

Table 1
Table detailing the sources used with the two different sized scintillators in this work.

Source	Moderation – Bonner sphere size (cm)	Number of accepted pulses
^{252}Cf	12.7	117,829
^{241}AmBe	None	54,306
^{241}AmBe	20.32	70,141

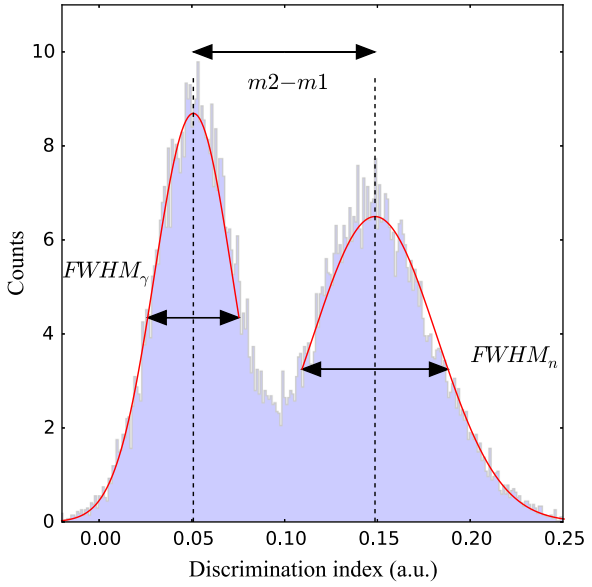

Fig. 3. Derivation of the figure of merit (FOM) calculations carried out in this work. The full width at half maximum (FWHM) is found for both the gamma events (the left hand distribution) and neutron events (the right hand distribution). The peak separation of the two normal distributions is divided by the sum of these two FWHM values.

3.1. Figure of merit

The quality of separation between neutron and gamma induced pulses in the scintillator can be quantified with a figure of merit (FOM) calculation shown as:

$$FOM = \frac{m2 - m1}{FWHM_n + FWHM_\gamma}, \quad (2)$$

where *m2* and *m1* are the corresponding discrimination index for neutron and gamma peaks from a normal distribution fitting of the data and FWHM is the full-width at half-maximum of each of these distributions. An example is shown in Fig. 3.

In this work two principal energy ranges were investigated in terms of neutron/gamma separation FOM. The first was 400–1300 keVee, the second was 300–400 keVee, this second region specifically focuses on the thermal neutron capture energy range. Using the mixtures function within the Python library, *scikit-learn*, normal distributions were fit to each of the peaks [25]. To check the quality of these fits a linear regression test was performed between the fit and experimental data. The lowest *r*-squared value observed was 0.986.

4. Results

4.1. Energy calibration

An energy calibration was performed on the system using two gamma sources, ^{22}Na and ^{137}Cs. An ^{22}Na source produces two gamma rays of energy 511 and 1275 keV, with corresponding Compton edges of 341 and 1062 keV, for gamma interactions in the scintillator. The ^{137}Cs produces 662 keV gamma rays with a corresponding Compton edge of 477 keV for gamma interactions. The ^{22}Na gamma source consisted of a 1 mm diameter ion exchange bead at the centre of a solid plastic disc 3 mm thick and 25 mm in diameter. The source was positioned 12 cm from the front face of the scintillator, 51,061 pulses were recorded. The ^{137}Cs source was located 1 m away from the front of the scintillator and 66,436 pulses were recorded. The raw pulse height data were compiled into a histogram counting the number of occurrences of

each ADC bit in the data as shown in Fig. 4. The Compton edges were found by taking the 75% value after each of the Compton peaks [26]. These three Compton edges are plotted in the inset of Fig. 4 and are shown to exhibit good linearity.

4.2. Raw data and filtering

To investigate the noise of the system, 100 raw pulses randomly selected from the ^{22}Na source irradiation were normalised to unit pulse height and are shown in Fig. 5. The blue shaded areas in Fig. 5(a) and (b) represent the maximum and minimum values of each sample bit, respectively. From inspection of the baseline in Fig. 5(a) it can be seen that below 200 keVee, relative to the peak of the pulse, the noise levels are reasonably high. As the energy increases towards the anticipated thermal capture region, between 300 and 400 keVee, Fig. 5(b) shows that this noise becomes less of a problem. However it can still be seen that due to sampling every 2 ns, by taking the maximum value recorded in each pulse there is potentially up to 2 ns jitter relative to the true peak. For the 300–400 keVee energy region, the blue shaded area after the peak from 20 to 25 ns is due to this jitter rather than noise.

4.3. Charge comparison method (CCM)

In this work the long (entire pulse) and short (tail of the pulse) integrals of each pulse have been found by summing the ADC samples within the temporal windows of their definitions. More computationally intensive methods of numerical integration have been shown to have no benefit when applied to CCM [10]. With each of the PSD techniques investigated in this work, parameters can be changed to optimise performance. In the case of CCM the short integral length can be optimised.

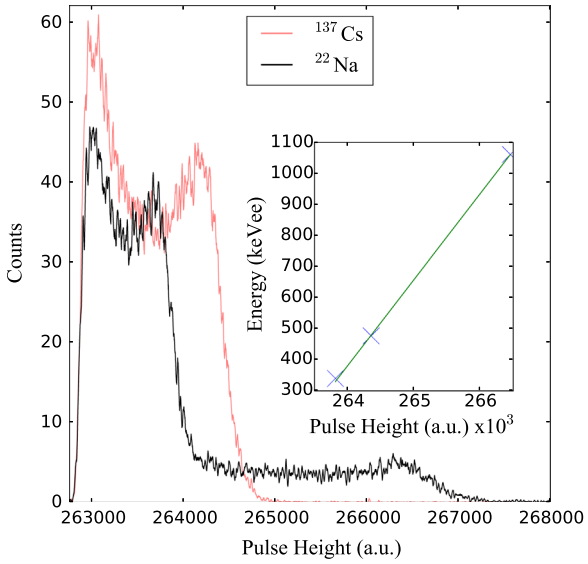

Fig. 4. Light output from two gamma emitting sources, ^{22}Na and ^{137}Cs, showing three Compton edges. These Compton edges of 341, 477 and 1062 keV are then translated to a pulse height. The inset shows the linearity of the calibration line intersecting these three points.

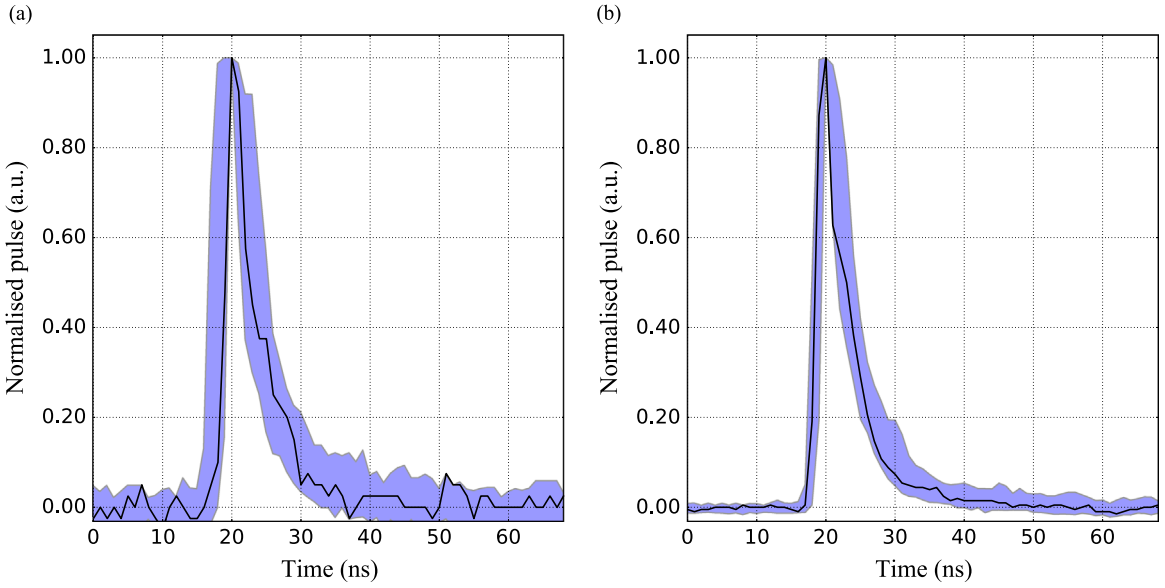

Fig. 5. Normalised raw pulse data recorded with ^{22}Na source. The black line shows a single raw pulse. For each sample bit, a maximum and minimum value in the data was recorded. These maximum and minimum values are the upper and lower bounds of the blue shaded area respectively for (a) pulses in the 100–200 keVee range, (b) pulses in the 300–400 keVee range. (For interpretation of the references to colour in this figure caption, the reader is referred to the web version of this paper.)

For a number of short integral lengths, the FOM was evaluated (using data obtained from an ^{241}AmBe source in the 800–1300 keVee range). The optimum value after the peak of the pulse to start the short integral was found to be 30 ns. This optimisation is shown in Fig. 6(a). The long integral was defined as 10 ns before the peak of the pulse to 140 ns after the peak of the pulse. Whilst these values are optimal for achieving the best figure of merit in this work, a trade off could be realised by reducing the length of the long integral to reduce pulse pile up problems. However in this work pulses have simply been rejected by a pile up algorithm. This algorithm rejected the data if two peaks occurred in a data packet (256 ns).

The performance of CCM with the ^{6}Li loaded scintillator can be seen in Fig. 6. In each of the figures, above 300 keVee, the gammas are found between a discrimination index of around −0.05 to 0.07. Above this, in the second plume, are the fast neutrons. Within this plume at around 340 keVee the thermal neutrons are found.

A high thermal, low fast neutron field was established using a 12.7 cm Bonner sphere around a ^{252}Cf source. The results are shown in Fig. 6(b). A low number of fast neutrons were observed, compared to numbers of thermal neutron captures. A high gamma contribution to this field can be seen and at the lower end of the thermal neutron region, at around 250 keVee. It can be seen that the discrimination between thermal neutrons and gammas becomes very difficult.

With a low thermal neutron content in an ^{241}AmBe field reasonable neutron/gamma discrimination can be observed down to around 500 keVee, as shown in Fig. 6(c). Below this energy, the uncertainty of an event being a neutron or gamma will be high.

4.4. Triangular filtering algorithm (TFA)

In this method a triangular filter is employed on the pulse and the difference in amplitude in output of the filter is used to discriminate between neutron and gamma events [18]. This discrimination takes place on a modified pulse consisting of only samples after the pulse peak, where each sample in this region is subtracted from the peak amplitude of the pulse. The recursive triangular filter formula is shown as

$$z[n] = z[n-1] + y[n] - 2y[n-k] + y[n-2k] \quad (3)$$

where z is the filtered pulse, y is the modified pulse (pulse from peak onwards), n is the current sample bit and k is an integer for the time constant of the filter. It should be noted that these pulses were also processed by additional filtering before being passed to the triangular filter. Savitzky–Golay, moving average and FIR filtering were investigated [27]. The highest FOM was observed with a 31 sample point moving average filter. With this optimised moving average filter, k was then varied to investigate the dependence of k on the FOM, and this optimisation is shown in Fig. 7(a). The peak value of the moving average filter was divided by the peak value of the triangular filter to find the discrimination index.

The parameter k selected for the results presented in this work was found by inspecting the FOM of the data obtained from an ^{241}AmBe source, specifically with data in the 800–1300 keVee range. A value of 67 was chosen for k. The results of the PSD performance can be seen in Fig. 7. It can be seen that very similar results to CCM were obtained.

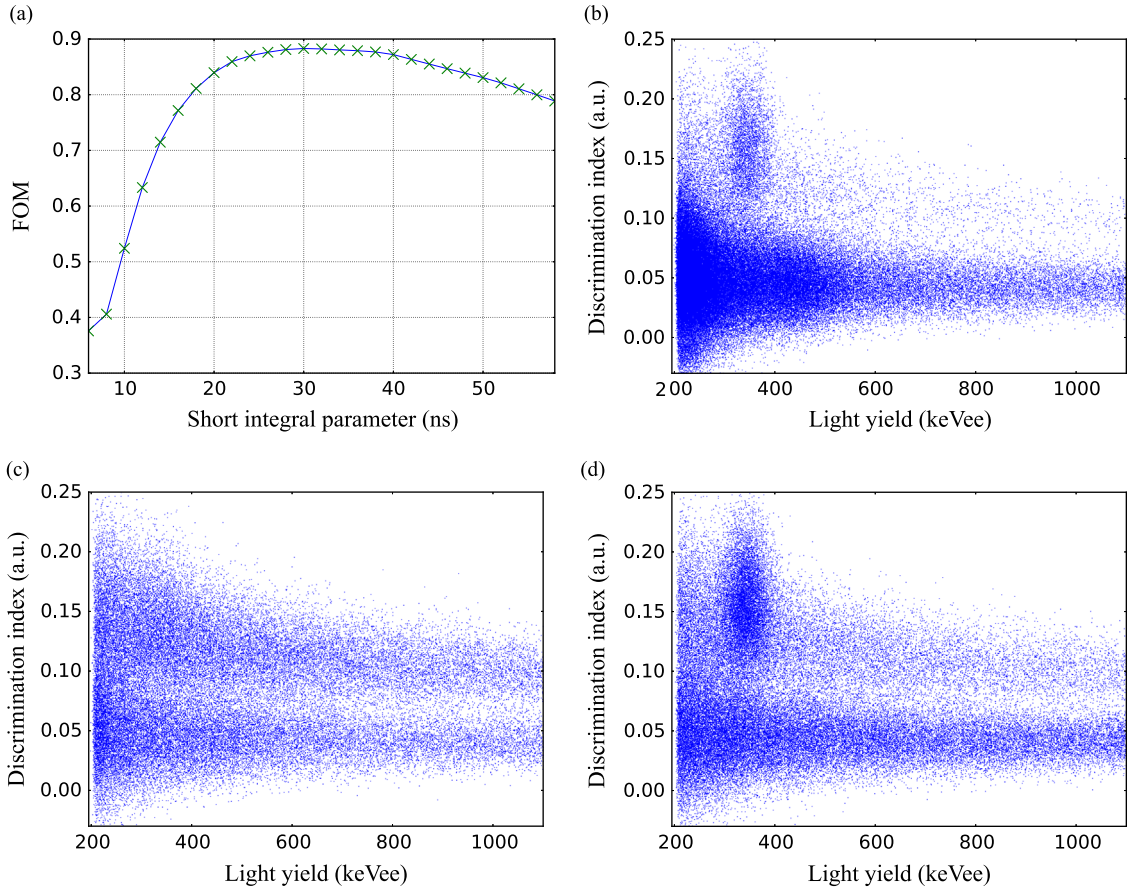

Fig. 6. Pulse shape discrimination results from charge comparison method (CCM). By varying the short integral length and evaluating the FOM, it was found that there was an (a) optimised short integral parameter. Long integral divided by short integrals versus the total light output for CCM pulse shape discrimination, with sources (b) moderated ^{252}Cf, (c) ^{241}AmBe, (d) moderated ^{241}AmBe.

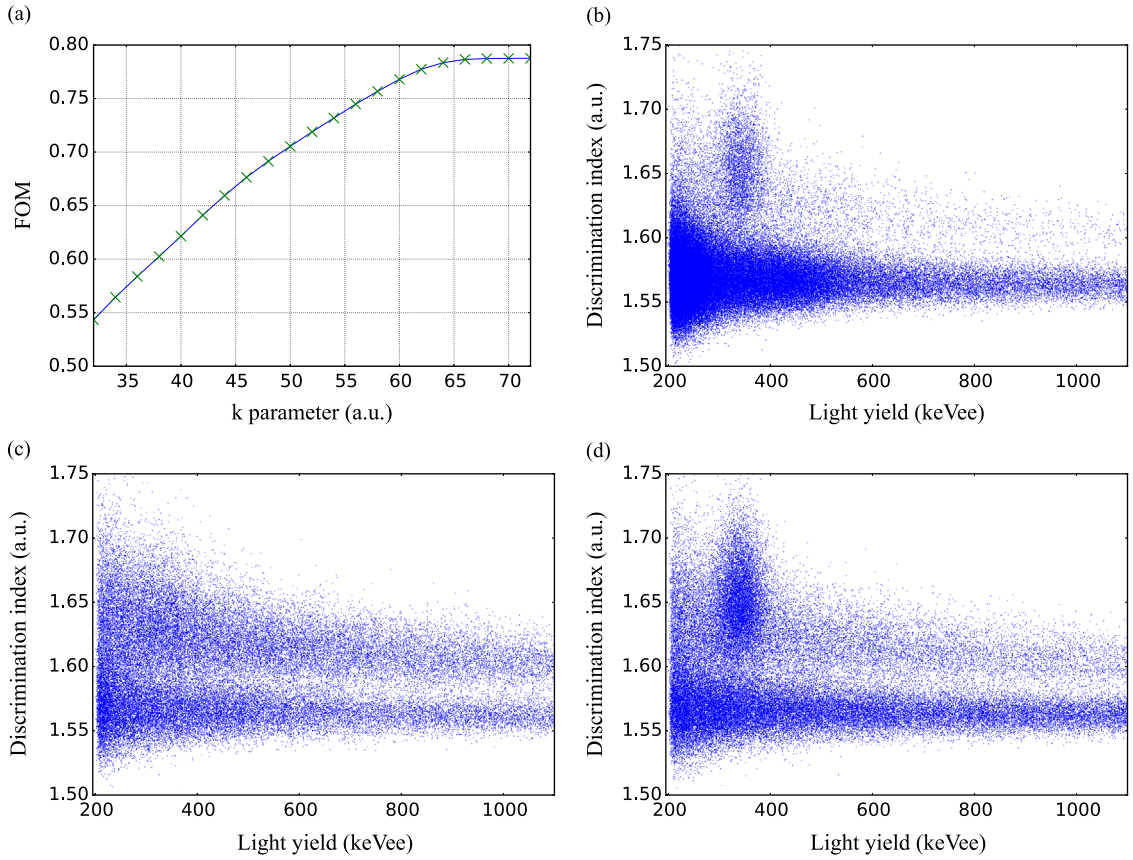

Fig. 7. Pulse shape discrimination results from triangular filtering algorithm (TFA). The optimisation of filter parameter *k* was performed by inspecting the resulting FOM for each value investigated (a). Normalised triangular filter output versus the total light output, with sources (b) moderated ^{252}Cf, (c) ^{241}AmBe, (d) moderated ^{241}AmBe.

4.5. Frequency gradient analysis (FGA)

Frequency gradient analysis is achieved by performing a Fast Fourier Transform (FFT) on the pulse [28]. Lui et al. have performed further optimisation of this technique involving the use of a moving average filter and an optimised discrimination parameter [29]. This optimised parameter is shown as

$$D_{fft} = 1 - \frac{|X[0]|}{|X[1]|} \tag{4}$$

where $X[0]$ and $X[1]$ are the first and second components of the FFT respectively.

In the empirical optimisation of the FGA method the baseline was removed from the pulse. This baseline was found by taking the average amplitude of the pulse in the range, *n-40* to *n-10*, where *n* is the ADC sample containing the pulse peak. Previous literature has discussed the use of a moving average filter with the FGA algorithm [29]. In this instance, it was found that optimal results were achieved without the use of a moving average filter. Furthermore, modifying the pulse to only consist of 10 ns before the peak and number of samples after the peak was found to bring further optimisation. The optimal value was found to be a 174 ns (87 sample bits) long segment of data after the pulse peak as shown in Fig. 8(a).

The FOM for the data can be seen in Table 2. For both fast only and thermal regions, it can be seen that with an unmoderated ^{241}AmBe field, for detection of fast neutrons in the 400–1300 keVee region (as well as the thermal neutron region of 300–400 keVee), FGA and CCM perform slightly better than TFA in terms of discriminating between neutron and gamma events. This trend was observed for ^{241}AmBe, ^{241}AmBe with a 20.32 cm Bonner sphere and ^{252}Cf with a 12.7 cm Bonner sphere.

5. Conclusion

Using a ^{6}Li loaded plastic scintillator, three pulse shape discrimination methods were investigated: FGA, TFA and CCM, with the primary aim of separating fast neutron and gamma events. Mixed radiation fields with thermal neutron content were also considered, and the ability of the three algorithms to discriminate these thermal events from gammas in the ^{6}Li loaded plastic scintillator was also investigated.

To describe the separation between neutron (fast and thermal) and gamma events, the quality of separation was quantified using a FOM. Two different energy regions were investigated in terms of FOM, 400–1300 keVee (fast neutron region) and 300–400 keVee (thermal neutron region). Although all three methods qualitatively perform very similarly, numerical analysis of the FOM showed that CCM was marginally better than FGA, where FGA was better than TFA in neutron/gamma separation in a ^{6}Li loaded plastic scintillator.

The optimisations for FGA and TFA found in this work are relevant for a 500 Msps, 11 bit digitiser, where previous experimental work with these algorithms was performed with lower resolution, faster sampling rate digitisers. Recent research has investigated differing sampling rates and resolutions [30,31]. Expanding on this work, repeating the methodology outlined in this paper for sample rates between 500 Msps and 4 Gsps and differing resolutions would further improve the understanding of the relative performance of the algorithms discussed in this work.

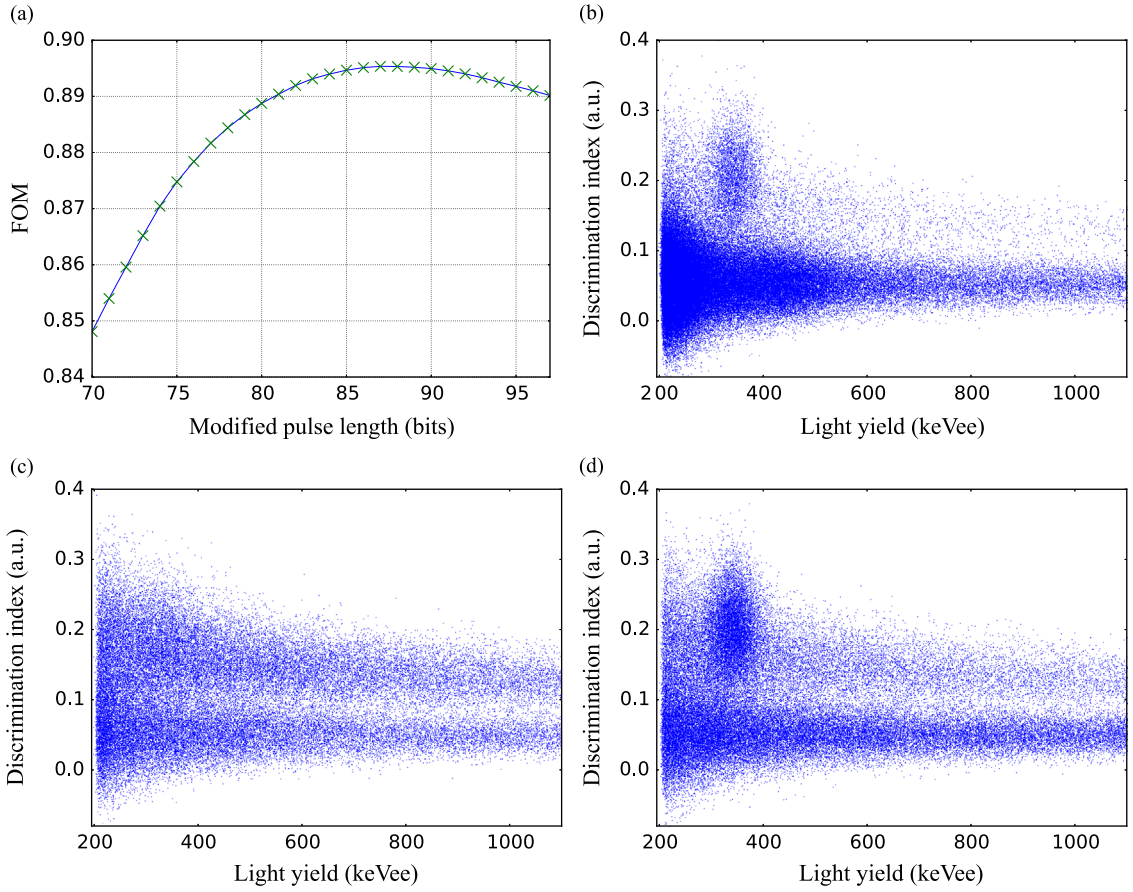

Fig. 8. Pulse shape discrimination results from frequency gradient analysis (FGA). The optimised length to sample after the peak was found in investigating a number of different lengths and inspecting the resulting FOM (a). Gradient between first and second components of FFT of the pulse versus the total light output for FGA pulse shape discrimination, with sources (b) moderated ^{252}Cf, (c) ^{241}AmBe, (d) moderated ^{241}AmBe.

Table 2
Figure of merit (FOM) for data presented in this work for CCM, FGA and TFA methods.

Energy Region	Source	Moderation	PSD Method	FOM
400–1300	^{241}AmBe	None	CCM	0.761
			FGA	0.766
			TFA	0.746
300–400	^{241}AmBe	None	CCM	0.660
			FGA	0.653
			TFA	0.625
300–400	^{241}AmBe	20.32 cm Bonner sphere	CCM	0.790
			FGA	0.773
			TFA	0.765
300–400	^{252}Cf	12.7 cm Bonner sphere	CCM	0.723
			FGA	0.694
			TFA	0.634

Recent research has also compared different pulse shaping algorithms [32]. Optimum filters for each PSD technique could also be further investigated with differing ADC sample rates and resolutions.

When comparing CCM and FGA it could be argued that although similar performance was observed between the two in terms of both fast and thermal neutron discrimination from gammas, the simplicity of CCM could be advantageous. However, with FPGA technology the number logic cells available is ever increasing. Thus the need for comparison of simplicity/processing time between PSD techniques becomes less of a salient point.

Acknowledgements

The authors would like to express thanks to Natalia Zaitseva and the team at LLNL for providing the scintillator sample. The authors would like to acknowledge the funding support from EPSRC and the National Physical Laboratory, Teddington, UK. We also acknowledge the help and advice of Dr. Nigel Hawkes at National Physical Laboratory. The authors acknowledge the use of the package Matplotlib for all plots in this research [33].

References

[1] N. Zaitseva, A. Glenn, H. Paul Martinez, L. Carman, I. Pawełczak, M. Faust, S. Payne, Nuclear Instruments and Methods in Physics Research Section A: Accelerators, Spectrometers, Detectors and Associated Equipment 729 (November) (2013) 747.
[2] G.F. Knoll, Radiation Detection and Measurement, 4th Edition, John Wiley & Sons, New York, 2010.
[3] F.D. Brooks, Nuclear Instruments and Methods 4 (3) (1959) 151.
[4] T.K. Alexander, F.S. Goulding, Nuclear Instruments and Methods 13 (1961) 244.
[5] M.L. Roush, M.A. Wilson, W.F. Hornyak, Nuclear Instruments and Methods 31 (1) (1964) 112.
[6] Jun Yang, Xiao-Liang Luo, Guo-Fu Liu, Cun-Bao Lin, Yan-Ling Wang, Qing-Qing Hu, Jin-Xian Peng, Chinese Physics C 36 (June (6)) (2012) 544.
[7] M. Flaska, S.A. Pozzi, Nuclear Instruments and Methods in Physics Research Section A: Accelerators, Spectrometers, Detectors and Associated Equipment 599 (February (2–3)) (2009) 221.
[8] S.D. Jastaniah, P.J. Sellin, Nuclear Instruments and Methods in Physics Research Section A: Accelerators, Spectrometers, Detectors and Associated Equipment 517 (January (1–3)) (2004) 202.
[9] G. Liu, M.D. Aspinall, X. Ma, M.J. Joyce, Nuclear Instruments and Methods in Physics Research Section A: Accelerators, Spectrometers, Detectors and Associated Equipment 607 (August (3)) (2009) 620.

[10] M. Nakhostin, Nuclear Instruments and Methods in Physics Research Section A: Accelerators, Spectrometers, Detectors and Associated Equipment 672 (April) (2012) 1.
[11] B. D'Mellow, M.D. Aspinall, R.O. Mackin, M.J. Joyce, A.J. Peyton, Nuclear Instruments and Methods in Physics Research Section A: Accelerators, Spectrometers, Detectors and Associated Equipment 578 (July (1)) (2007) 191.
[12] S. Märrone, D. Cano-Ott, N. Colonna, C. Domingo, F. Gramegna, E.M. Gonzalez, F. Gunsing, M. Heil, F. Kppeler, P.F. Mastinu, Nuclear Instruments and Methods in Physics Research Section A: Accelerators, Spectrometers, Detectors and Associated Equipment 490 (1) (2002) 299.
[13] N.P. Hawkes, K.A.A. Gamage, G.C. Taylor, Radiation Measurements 45 (December (10)) (2010) 1305.
[14] T. Tambouratzis, D Chernikova, I. Pazsit, A comparison of artificial neural network performance: the case of neutron/gamma pulse shape discrimination, in: 2013 IEEE Symposium on Computational Intelligence for Security and Defense Applications (CISDA), 2013, pp. 88–95.
[15] T.S. Sanderson, C.D. Scott, M. Flaska, J.K. Polack, S.A. Pozzi, Machine learning for digital pulse shape discrimination, in: 2012 IEEE Nuclear Science Symposium and Medical Imaging Conference (NSS/MIC), IEEE, Anaheim, CA, 2012, pp. 199–202.
[16] D. Savran, B. Löher, M. Miklavec, M. Vencelj, Nuclear Instruments and Methods in Physics Research Section A: Accelerators, Spectrometers, Detectors and Associated Equipment 624 (December (3)) (2010) 675.
[17] S.D. Ambers, M. Flaska, S.A. Pozzi, Nuclear Instruments and Methods in Physics Research Section A: Accelerators, Spectrometers, Detectors and Associated Equipment 638 (May (1)) (2011) 116.
[18] M. Nakhostin, Journal of Instrumentation 8 (May (05)) (2013) P05023.
[19] V. Esmaeili-sani, A. Moussavi-zarandi, N. Akbar-ashrafi, B. Boghrati, H. Afarideh, Nuclear Instruments and Methods in Physics Research Section A: Accelerators, Spectrometers, Detectors and Associated Equipment 694 (December) (2012) 113.
[20] Shiping Li, Xiufeng Xu, Hongrui Cao, Guoliang Yuan, Qing-wei Yang, Zejie Yin, Applied Radiation and Isotopes 72 (February) (2013) 30.
[21] D.I. Shippen, M.J. Joyce, M.D. Aspinall, IEEE Transactions on Nuclear Science NS-57 (October (5)) (2010) 2617.
[22] G. Liu, J. Yang, X.L. Luo, C.B. Lin, J.X. Peng, Y. Yang, Radiation Measurements 58 (November) (2013) 12.
[23] S. Yousefi, L. Lucchese, M.D. Aspinall, Nuclear Instruments and Methods in Physics Research Section A: Accelerators, Spectrometers, Detectors and Associated Equipment 598 (January (2)) (2009) 551.
[24] X.L. Luo, Y.K. Wang, J. Yang, G. Liu, C.B. Lin, Q.Q. Hu, J.X. Peng, Nuclear Instruments and Methods in Physics Research Section A: Accelerators, Spectrometers, Detectors and Associated Equipment 717 (July) (2013) 44.
[25] F. Pedregosa, G. Varoquaux, A. Gramfort, V. Michel, B. Thirion, O. Grisel, M. Blondel, P. Prettenhofer, R. Weiss, V. Dubourg, J. Vanderplas, A. Passos, D. Cournapeau, M. Brucher, M. Perrot, E. Duchesnay, Journal of Machine Learning Research 12 (2011) 2825.
[26] A.A. Naqvi, H. Al-Juwair, K. Gul, Nuclear Instruments and Methods in Physics Research Section A: Accelerators, Spectrometers, Detectors and Associated Equipment 306 (12) (1991) 267.
[27] M.U.A. Bromba, H. Ziegler, Analytical Chemistry 53 (11) (1981) 1583.
[28] G. Liu, M.J. Joyce, X. Ma, M.D. Aspinall, IEEE Transactions on Nuclear Science NS-57 (June (3)) (2010) 1682.
[29] Guo-Fu Liu, Luo Xiao-Liang, Jun Yang, Cun-Bao Lin, Qing-Qing Hu, Jin-Xian Peng, Chinese Physics C 37 (June (6)) (2013) 066201.
[30] D. Cester, M. Lunardon, G. Nebbia, L. Stevanato, G. Viesti, S. Petrucci, C. Tintori, Nuclear Instruments and Methods in Physics Research Section A: Accelerators, Spectrometers, Detectors and Associated Equipment 748 (June) (2014) 33.
[31] C. Hellesen, M. Skiba, G. Ericsson, E. Andersson Sundén, F. Binda, S. Conroy, J. Eriksson, M. Weiszflog, Nuclear Instruments and Methods in Physics Research Section A: Accelerators, Spectrometers, Detectors and Associated Equipment 720 (August) (2013) 135.
[32] J. Kamleitner, S. Coda, S. Gnesin, Ph. Marmillod, Nuclear Instruments and Methods in Physics Research Section A: Accelerators, Spectrometers, Detectors and Associated Equipment 736 (February) (2014) 88.
[33] J.D. Hunter, Computing in Science and Engineering 9 (3) (2007) 90.